Effects of geometrical ray chaos on the electromagnetic eigenmodes of a gradient index optical cavity

P. B. Wilkinson,[1] T. M. Fromhold,[1] R. P. Taylor,[2] and A. P. Micolich[2]
[1]*School of Physics and Astronomy, University of Nottingham, Nottingham NG7 2RD, United Kingdom*
[2]*Physics Department, University of Oregon, Eugene, Oregon 97403-1274*
(Received 3 May 2001; published 16 July 2001)

Electromagnetic analogies of quantum chaos are investigated in two-dimensional optical cavities which have reflective surfaces and contain a gradient refractive index medium. As the shape of the cavity is transformed continuously from a rectangle to a parallelogram, the geometrical ray paths undergo a transition from stable to chaotic dynamics. In the chaotic regime, the spectral statistics of the cavity are accurately described by random matrix theory. In addition, the electromagnetic mode spectrum of the cavity is modulated by both real and ghost periodic ray paths. These paths also ''scar'' the electric field intensity distributions of regular subsets of cavity eigenmodes.

DOI: 10.1103/PhysRevE.64.026203 PACS number(s): 05.45.Mt, 42.65.Sf

I. INTRODUCTION

Several key advances in the understanding of quantum chaos have resulted from the study of billiard systems, in which a particle is confined in a two-dimensional (2D) potential well. For example, wave functions which are ''scarred,'' having a high concentration of probability density along an unstable but periodic classical orbit, were first identified in numerical studies of the stadium billiard [1]. They were subsequently detected in experiments on both 2D stadium-shaped microwave cavities [2] and semiconductor quantum dots [3]. Wave function scarring also has a pronounced effect on the current–voltage $I(V)$ characteristics of resonant tunneling diodes (RTD's) containing a wide quantum well in a tilted magnetic field [4]. In the RTD's, the hard walls of the quantum well and the parabolic potential (which corresponds to the magnetic field) form an unusual 2D billiard with chaotic electron dynamics. This type of billiard supports a hierarchy of unstable and stable periodic orbits. But the electron scattering rate due to longitudinal optical phonon emission is so high that $I(V)$ measurements can only resolve quantized states corresponding to a few of the shortest periodic orbits [4].

In this paper, we analyze in detail the geometrical ray dynamics and electromagnetic eigenmodes of a chaotic optical cavity. The cavity, a parallelogram with reflective surfaces and gradient refractive index (GRIN) interior, supports ray dynamics and eigenmodes analogous to those of an electron in the RTD. In previous work [5] we showed that these properties of the cavity should be accessible to laser transmission experiments, with the advantage that the long coherence length of laser light will give very high resolution. In particular, for a cavity with semisilvered (partially transmitting) end surfaces, the transmission coefficient should exhibit a series of sharp resonant peaks as a function of laser frequency. These peaks are associated with the eigenmodes of the closed cavity (fully reflective surfaces) and the underlying dynamics of its geometrical ray paths. Here we present a detailed analysis of the spectral fluctuations and scarred modes associated with the chaotic ray dynamics of the closed cavity.

We consider a 2D parallelogram cavity with perfectly reflecting walls, containing a dielectric material with a spatially varying refractive index profile [Fig. 1(a)]. Such a cavity could be made for planar ''meridional'' rays [6] by silvering the sides and angled ends of a commercially available gradient index lens [5]. Based on a real lens [7], the index profile of the cavity studied in this paper is $n(y) = n_0(1-\alpha^2 y^2)^{1/2}$, where $n_0 = 1.5$, $\alpha = 608.84\ \mathrm{m}^{-1}$ and y is the radial distance from its axis [Fig. 1(b)]. Its length and diameter are $L = 2.58\times10^{-3}$ m and $W = 10^{-3}$ m, respectively.

II. GEOMETRICAL OPTICS

The geometrical ray paths in an optical medium with an arbitrarily varying refractive index are determined by the ray equation [8]

$$\frac{d}{ds}\left(n\frac{d\mathbf{r}}{ds}\right) = \nabla n, \tag{1}$$

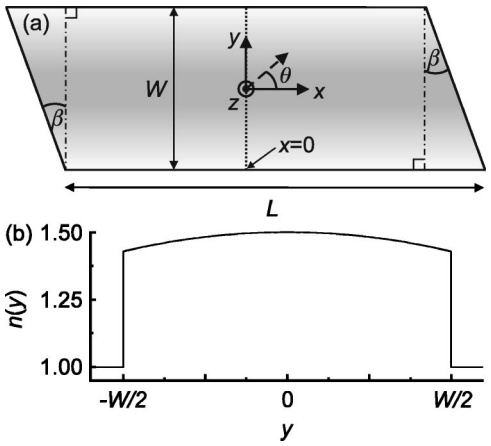

FIG. 1. (a) Schematic diagram of the 2D closed gradient index cavity showing the tilt angle β of the planar ends. The dashed line shows the direction of the ray path at $x=0$ (dotted line) relative to the x and y axes. The gray-scale shading shows the refractive index variation (gray high, white low). (b) The refractive index profile $n(y)$.

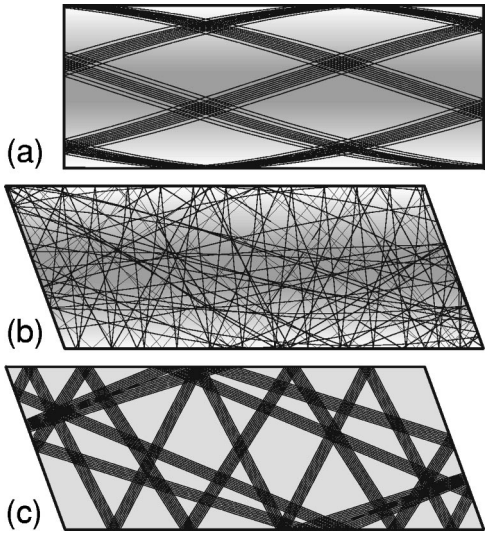

FIG. 2. Typical geometrical ray paths in (a) a stable GRIN cavity with $\beta=0°$; (b) a chaotic GRIN cavity with $\beta=20°$; and (c) a pseudointegrable constant index cavity with $\beta=20°$.

where $\mathbf{r}$ is a position vector and s is a displacement along the ray path. This equation can be rewritten as

$$\frac{d^2\mathbf{r}}{dq^2}=n\nabla n, \tag{2}$$

where $d/dq=nd/ds$. For the refractive index profile $n(y)$ given above, the x and y components of Eq. (2) are

$$\frac{d^2x}{dq^2}=0 \tag{3}$$

and

$$\frac{d^2y}{dq^2}=-n_0^2\alpha^2y, \tag{4}$$

respectively. The rays described by Eqs. (3) and (4) follow sinusoidal paths inside the cavity but undergo specular reflection at the silvered surfaces. The geometrical ray paths therefore consist of sinusoidal path segments linked by reflections which occur at regular or irregular time intervals depending on the tilt angle β of the angled end surfaces [Fig. 1(a)]. When $\beta=0°$, the cavity is rectangular and the ray paths are reflected at regular intervals and are stable [Fig. 2(a)]. But when $\beta\neq0°$, the angled end surfaces interrupt the regular sinusoidal path segments at irregular times, generating chaotic ray dynamics [Fig. 2(b)]. The combination of a smooth refractive index profile (analogous to the effective parabolic potential for an electron in a magnetic field [4]) and an impenetrable boundary wall makes an interesting hybrid system that has characteristics of both the RTD and more traditional flat-bottomed 2D billiards.

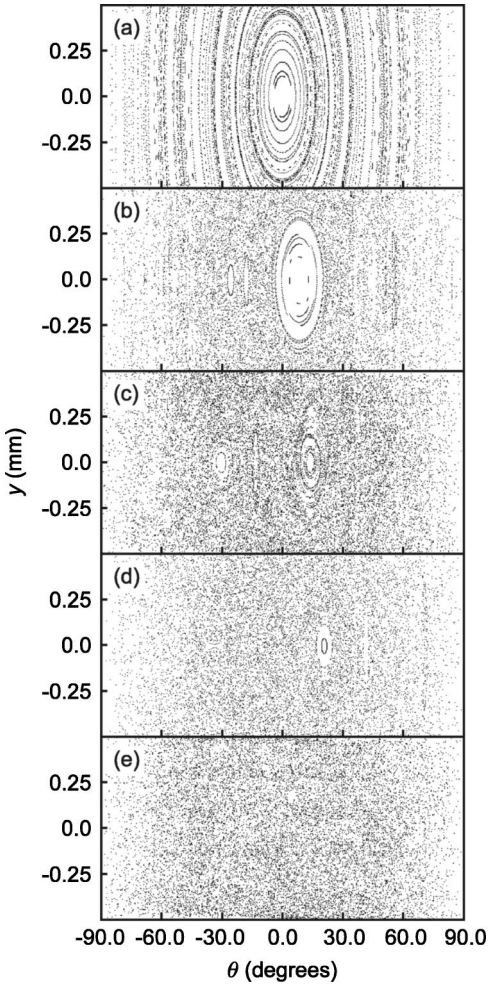

FIG. 3. Poincaré sections showing coordinates (θ,y) for rays crossing the plane $x=0$ traveling from left to right in Fig. 1(a): (a) $\beta=0°$, (b) $\beta=5°$, (c) $\beta=10°$, (d) $\beta=15°$, and (e) $\beta=20°$.

In the parallelogram cavity, the GRIN material is essential for creating the chaotic ray paths. This is in contrast with previous studies of chaotic rays in deformed optical fibers with a constant refractive index [9]. Without the index variation, polygonal 2D billiards either belong to the class of ''pseudointegrable'' systems (if at least one interior angle is a rational multiple of π, like our parallelogram) or ''ergodic'' systems (if all interior angles are irrational multiples of π). In general the characteristics of the classical dynamics of pseudointegrable systems are closer to those of integrable (stable) systems than chaotic systems. Figure 2(c) shows a typical ray path in a pseudointegrable parallelogram cavity. It is important to note that, in common with the stable case shown in Fig. 2(a), neighboring paths do not exhibit exponential divergence. Therefore neither of these systems generate chaotic dynamics [10], instead both support nonisolated families of stable ray paths. This is in contrast to the chaotic and isolated periodic ray paths which exist in the GRIN cavity shown in Fig. 2(b).

To quantify the transition from stable to chaotic dynamics, Fig. 3 shows Poincaré sections (slices through phase space) for tilt angles $0°\leqslant\beta\leqslant20°$. The sections are generated by

plotting the variables θ and y (see Fig. 1) each time the ray path intersects the line $x=0$ with $dx/dt>0$. At $\beta=0°$, the points lie on concentric elliptical rings [Fig. 3(a)] showing that the ray paths are stable. As β is increased to 5°, 10° and 15° [Figs. 3(b)–3(d)] the phase space reveals progressively shrinking, isolated KAM islands of stability [11] embedded in a chaotic sea. When $\beta=20°$ [Fig. 3(e)] the phase space is almost completely chaotic, and contains very few stable islands, which are too small to show up in the figure.

III. SOLVING THE WAVE EQUATION

In quantum chaos, there are strong connections between the eigenenergies and eigenstates of the quantum system and the periodic trajectories of its chaotic classical counterpart. Experimental studies of quantum chaotic systems have been made using 2D microwave billiard cavities, which have exploited the formal identity of the Schrödinger equation and electromagnetic wave equation [2]. Similarly we consider the effects of chaotic ray dynamics in the GRIN cavity on its electromagnetic modes. In a 2D system, there are two mutually orthogonal polarizations of the electromagnetic waves; either the electric field **E** or the magnetic field **H** is perpendicular to the plane of the cavity. These field orientations are called the transverse magnetic (TM) and transverse electric polarizations, respectively. In this paper we consider TM modes, since they obey Dirichlet boundary conditions ($E=0$) on the perfectly reflecting cavity walls, identical to the boundary conditions for wave functions in a hard-walled quantum billiard. The modes obey the Maxwell equations

$$\nabla\times\mathbf{E}=-\frac{\partial\mathbf{B}}{\partial t} \tag{5}$$

and

$$\nabla\times\mathbf{H}=\frac{\partial\mathbf{D}}{\partial t}, \tag{6}$$

where $\mathbf{B}=\mu_r\mu_0\mathbf{H}$ and $\mathbf{D}=\epsilon_r\epsilon_0\mathbf{E}$. We assume that the cavity material is nonmagnetic ($\mu_r=1$) and has a refractive index profile $n^2(y)=\epsilon_r(y)$ [12]. We take the curl of Eq. (5) and substitute for $\nabla\times\mathbf{H}$ from Eq. (6) to obtain

$$\nabla\times\nabla\times\mathbf{E}=-\frac{n^2}{c^2}\frac{\partial^2\mathbf{E}}{\partial t^2}. \tag{7}$$

By expanding the vector triple product in Eq. (7) and substituting

$$\nabla\cdot\mathbf{E}=-\mathbf{E}\cdot\frac{\nabla n^2}{n^2}, \tag{8}$$

(which is derived from $\nabla\cdot\mathbf{D}=0$) we obtain the wave equation

$$\nabla^2\mathbf{E}-\frac{n^2}{c^2}\frac{\partial^2\mathbf{E}}{\partial t^2}=-\nabla\left(\mathbf{E}\cdot\frac{\nabla n^2}{n^2}\right). \tag{9}$$

In general, the term on the right-hand side of Eq. (9) couples the spatial components of **E**, causing the polarization of the wave to change with time. However, for TM modes in the 2D GRIN cavity, the coupling term is zero because **E** and ∇n^2 are orthogonal. For a time-harmonic field of angular frequency ω the nonzero field component $E_z(x,y)$ exactly obeys the scalar wave equation

$$\frac{\partial^2E_z}{\partial x^2}+\frac{\partial^2E_z}{\partial y^2}+k^2n^2E_z=0, \tag{10}$$

where $k=\omega/c$ is the free-space wave number. Equation (10) is analogous to the 2D Schrödinger equation. Discrete eigenmodes, analogous to quantum eigenstates, with wave numbers $k=k_j$ ($j=1,2,3,\ldots$) form within the cavity because E_z must vanish on its perfectly reflecting surfaces.

In our previous work on this system, we used a fourth-order accurate finite difference technique [13] to solve Eq. (10) for the refractive index profile of the GRIN lens. In this paper we use a different solution method which allows us to calculate eigenmodes at frequencies an order of magnitude higher than was possible using the finite difference method. This method is based on the plane wave decomposition (PWD) technique developed in studies of quantum chaos in billiard systems [14]. We write $E_z(x,y)=F(x)G(y)$ and separate Eq. (10) to yield

$$\frac{d^2F}{dx^2}+n_0^2k_x^2F=0 \tag{11}$$

and

$$\frac{d^2G}{dy^2}+[n_0^2k_y^2-n_0^2k^2\alpha^2y^2]G=0, \tag{12}$$

where $k_x^2+k_y^2=k^2$. The even and odd parity particular solutions of Eq. (11) are

$$F_e(x)=\cos(n_0k_xx) \tag{13}$$

and

$$F_o(x)=\sin(n_0k_xx), \tag{14}$$

respectively. Less trivially, the even and odd parity solutions of Eq. (12) are

$$G_e(y)=\exp\left(-\frac{n_0k\alpha}{2}y^2\right)\mathcal{F}\left[\frac{1}{4}-\frac{n_0k_y^2}{4k\alpha};\frac{1}{2};n_0k\alpha y^2\right], \tag{15}$$

and

$$G_o(y)=y\exp\left(-\frac{n_0k\alpha}{2}y^2\right)\mathcal{F}\left[\frac{3}{4}-\frac{n_0k_y^2}{4k\alpha};\frac{3}{2};n_0k\alpha y^2\right], \tag{16}$$

where $\mathcal{F}$ is any general solution of Kummer's equation [15]. A convenient particular solution is the confluent hypergeometric function ${}_1F_1$ which has the series expansion

$${}_1F_1[a;b;z]=\sum_{n=0}^{\infty}\frac{(a)_nz^n}{(b)_nn!}, \tag{17}$$

where $(a)_n=a(a+1)(a+2)\ldots(a+n-1)$.

The rotational symmetry of the cavity [see Fig. 1(a)] requires that its eigenmodes have one of two parities $E_{\pm}(x,y)=\pm E(-x,-y)$. Following the PWD method, we write these independent modes as expansions over combinations of Eqs. (13)–(16):

$$E_+(x,y)=\sum_{i=1}^{N}[u_iF_e(x)G_e(y)+v_iF_o(x)G_o(y)], \tag{18}$$

and

$$E_-(x,y)=\sum_{i=1}^{N}[u_iF_e(x)G_o(y)+v_iF_o(x)G_e(y)], \tag{19}$$

where $\{u_i\}$ and $\{v_i\}$ are expansion coefficients relating to k_{x_i} and k_{y_i}, respectively. For a given k and parity, N arbitrarily selected k_{x_i} and k_{y_i} pairs are chosen subject to the condition $k_{x_i}^2+k_{y_i}^2=k^2$, giving a total of $2N$ expansion coefficients. To find these coefficients we construct a matrix equation by considering $2N-1$ points around one rotationally symmetric half of the cavity perimeter [on which the Dirichlet boundary condition ensures $E(x,y)=0$] and one point within the cavity [where we choose $E(x,y)=1$]. The matrix is close to singular for useful values of N, so we solve the matrix equation by singular value decomposition [16]. The frequencies of the eigenmodes are found by calculating the "tension" $T=\Sigma_j|E(x_j,y_j)|^2$ [2,14] as a function of frequency at *intermediate* points (x_j,y_j) between the $2N-1$ points used in the matrix equation. The eigenfrequencies are found by searching for minima in T ($T=0$ at an exact eigenfrequency).

IV. ANALOGIES WITH QUANTUM CHAOS

To investigate the connections between the chaotic geometrical ray paths and the eigenmodes of the cavity, we have calculated the first 1000 modes using the above technique. The density of the eigenmodes $\rho(k)$ can be written

$$\rho(k)=\sum_j\delta(k-k_j)=\overline{\rho}(k)+\tilde{\rho}(k), \tag{20}$$

where $\overline{\rho}(k)$ is a smooth, monotonically increasing average density and $\tilde{\rho}(k)$ is the remaining fluctuating contribution. The average density is given by the Weyl formula [11] and, by analogy with quantum billiards containing a spatially varying potential [17], is given by

$$\overline{\rho}(k)=\frac{A\overline{n^2}}{2\pi}k-\frac{P\overline{n}}{4\pi}, \tag{21}$$

where A and P are the area and perimeter of the cavity, respectively, $\overline{n^2}$ is the mean of n^2 over A, and $\overline{n}$ is the mean of n over P. As with quantum chaotic systems, the frequency spacings between adjacent cavity eigenmodes are affected by the underlying dynamics of the geometrical ray paths. If the frequencies are scaled so that $\overline{\rho}(k)=1$ for all k then, for stable nonchaotic dynamics, random matrix theory predicts that the probability $P(s)ds$ of finding a scaled frequency spacing between s and $s+ds$ is given by the Poisson distribution. For time-reversible strongly chaotic dynamics, the scaled frequency spacings have a Gaussian orthogonal ensemble (GOE) distribution [11] given by

$$P(s)=\frac{\pi}{2}s\exp(-s^2\pi/4). \tag{22}$$

The solid curve in Fig. 4(a) shows the probability $N(S)=\int_0^SP(s)ds$ of finding a scaled level spacing $\leqslant S$ for the chaotic GRIN cavity with $\beta=20°$. The distribution closely follows the GOE prediction (dashed curve) for strongly chaotic systems. For comparison, $N(S)$ for the Poisson distribution is also shown (dot-dashed curve).

We have also calculated the first 1000 eigenmodes of a pseudointegrable cavity of the same dimensions but with a constant refractive index of $n=1.480\,07$ (this value was chosen such that $\overline{\rho}(k)$ for the pseudointegrable and chaotic cavities matched as closely as possible). The frequency spacings of pseudointegrable systems are not so well understood as those of strongly chaotic systems. Numerical studies [10] have shown that $P(s)$ in pseudointegrable systems follows a probability distribution intermediate between the integrable (Poisson statistics) and strongly chaotic (GOE statistics) cases. To quantify the level statistics of the pseudointegrable cavity we fit the observed distribution to the phenomenological distribution

$$P(s)=(d+1)C(d)s^d\exp[-C(d)s^{d+1}] \tag{23}$$

proposed by Brody [18]. The distribution parameter d can vary continuously between $d=0$ (Poisson statistics) and $d=1$ (GOE statistics), where $C(d)=[\Gamma([d+2]/[d+1])]^{d+1}$.

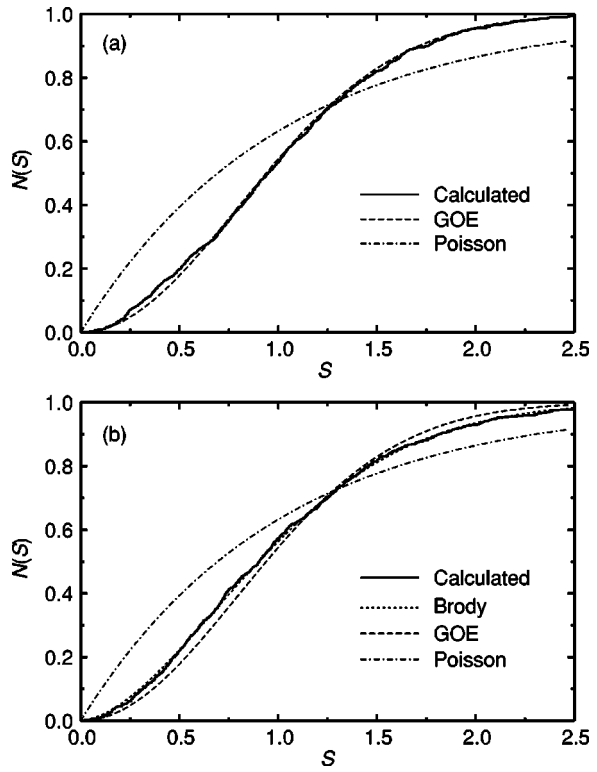

FIG. 4. Cumulative probability distributions $N(S)$ (solid curves) of finding a scaled frequency spacing $\leqslant S$ for: (a) the chaotic GRIN cavity and (b) the pseudointegrable constant index cavity. In (a) and (b) the GOE (dashed curve) and Poisson (dot-dashed curve) distributions are shown for comparison. In (b) the Brody distribution with $d=0.736$ (dotted curve) is also shown.

A least-squares fit of $N(S)$ for the pseudointegrable cavity to a Brody distribution [dotted curve in Fig. 4(b)] gives $d=0.736$. This indicates that without the GRIN material, the statistics of frequency spacings differ significantly from those associated with strongly chaotic systems ($d=1$).

The energy level spectra of quantum chaotic systems also exhibit *long range* correlations associated with the unstable periodic orbits of the corresponding classical system. The fluctuating part of the energy level density is given by the semiclassical trace formula (TF) for a quantum chaotic system [11]. By analogy with the TF, it follows that the contribution to $\tilde{\rho}(k)$ from an unstable periodic ray of optical path length Λ has a period of $\Delta\omega=2\pi c/\Lambda$ and an amplitude $F(\Lambda)$ given by the Fourier transform

$$F(\Lambda)\approx\int_0^{k_{\max}}\tilde{\rho}(k)U(k)\exp(-ik\Lambda)dk, \qquad (24)$$

where $k_{\max}$ is the wave number of the highest eigenmode considered and $U(k)$ is the Bartlett window function [16] which is used to suppress ringing in the Fourier transform. The power spectrum of $\tilde{\rho}(k)$ shown in the upper part of Fig. 5 is calculated for the first 1000 modes of the GRIN cavity and reveals a series of numbered peaks at Λ values equal to the optical path lengths of the periodic ray paths shown in

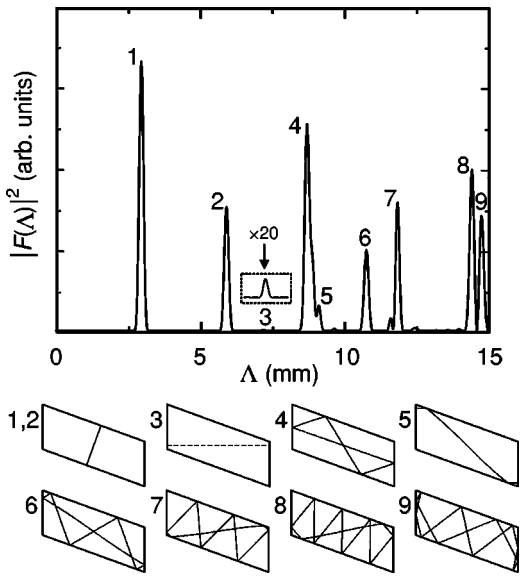

FIG. 5. Top: Fourier power spectrum of $\tilde{\rho}(k)$ as a function of optical path length Λ, showing numbered peaks. Inset box shows peak 3 vertically magnified by factor of 20. Bottom: Real (solid) and ghost (dashed) periodic ray paths which correspond to the peaks indicated by the numbers to the left of each path.

the lower part of the figure. The numbers to the left of each path specify the indices of the associated peaks in the Fourier power spectrum. In most quantum chaotic systems, the periods of the relevant unstable periodic orbits change with energy, broadening the peaks in the Fourier transform. By contrast, as the GRIN cavity is an optical system, the periods (path lengths) of the geometrical ray paths are independent of ω. This means that the widths of the peaks in $|F(\Lambda)|^2$ are limited only by the finite $k_{\max}$. This allows us to match the ray paths to the peaks very precisely (the discrepancy is $\lesssim 1\%$ for all peaks). Peaks 1 and 2 correspond, respectively, to single and double traversals of a simple ''bouncing-ball'' ray path across the cavity. There is a nonisolated family of these marginally stable paths which have previously been identified in chaotic stadium billiards [19]. Peaks 4–8 are associated with progressively more complicated unstable periodic ray paths involving multiple reflections from the cavity walls. Peak 9 corresponds to a stable periodic path. There is also an additional small, but isolated and distinct, peak 3 for which no periodic trajectory exists. This peak corresponds to a ''ghost'' [20] of the stable periodic ray path 3 which is found in the pseudointegrable cavity of the same shape with constant refractive index $n=1.480\,07$.

In addition to periodic fluctuations in the density of levels of a quantum chaotic system, unstable periodic orbits also cause enhancements of probability density (''scars'') along the orbit in groups of eigenstates [1–4]. An analogous effect, a concentration of electric field intensity along an unstable periodic ray path, occurs in many of the eigenmodes of the GRIN cavity. The frequency spacing between successive groups of eigenmodes scarred by a particular unstable periodic ray path of optical path length Λ equals the periodicity of the corresponding fluctuations in the density of modes $\Delta\omega=2\pi c/\Lambda$.

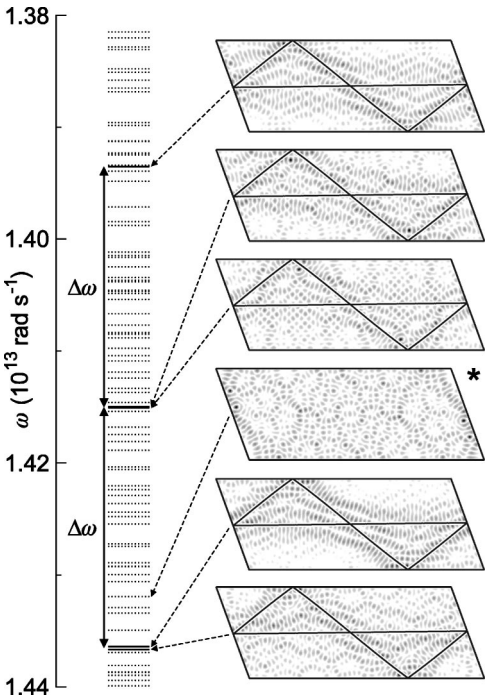

FIG. 6. Horizontal lines: eigenfrequencies of the chaotic cavity with $\beta = 20°$. The solid lines mark the frequencies of the scarred eigenmodes shown on the right of the figure. The scarring ray path is shown overlaid on the electric field intensity plots (white = 0, black = high) of each scarred mode. The spacing between each group of scarred modes is $\Delta\omega = 2.14\times10^{11}$ rad s^{-1}. The electric field intensity variation of an unscarred eigenmode (marked with an asterisk) is shown for comparison.

To illustrate this, Fig. 6 shows a sequence of eigenmodes which are scarred by the unstable periodic ray path labeled 4 in Fig. 5. For comparison, a nearby mode (marked with an asterisk) is also shown which reveals no trace of the scarring effect. The frequency spacing between each group of scarred modes, $\Delta\omega = 2.14\times10^{11}$ rad s^{-1}, agrees closely with the spacing of $\Delta\omega = 2.17\times10^{11}$ rad s^{-1} predicted from the optical path length of $\Lambda = 8.67$ mm.

To better identify scarred eigenmodes, we have calculated the Wigner function

$$\gamma(y,\theta) \propto \int E_z(\mathbf{r}+\mathbf{l})E_z(\mathbf{r}-\mathbf{l})\exp[-2ikn(\mathbf{r})\mathbf{s}\cdot\mathbf{l}]d\mathbf{l}, \tag{25}$$

which, for each mode, gives a phase space representation of the electric field distribution analogous to the classical Poincaré section [21]. In Eq. (25), $\mathbf{r} = (x,y)$, $\mathbf{l}$ is a displacement from $\mathbf{r}$ in the (x,y) plane and $\mathbf{s} = (\cos\theta, \sin\theta)$. The plots on the left-hand side of Fig. 7 show the electric field intensity distributions of five different eigenmodes. Each of these distributions is scarred by the unstable periodic ray path shown overlaid. The plots on the right-hand side show the Wigner functions of each scarred mode, which are calculated for $x = 0$ like the Poincaré sections in Fig. 3. The large positive values of γ (white) are centered on the initial coordinates

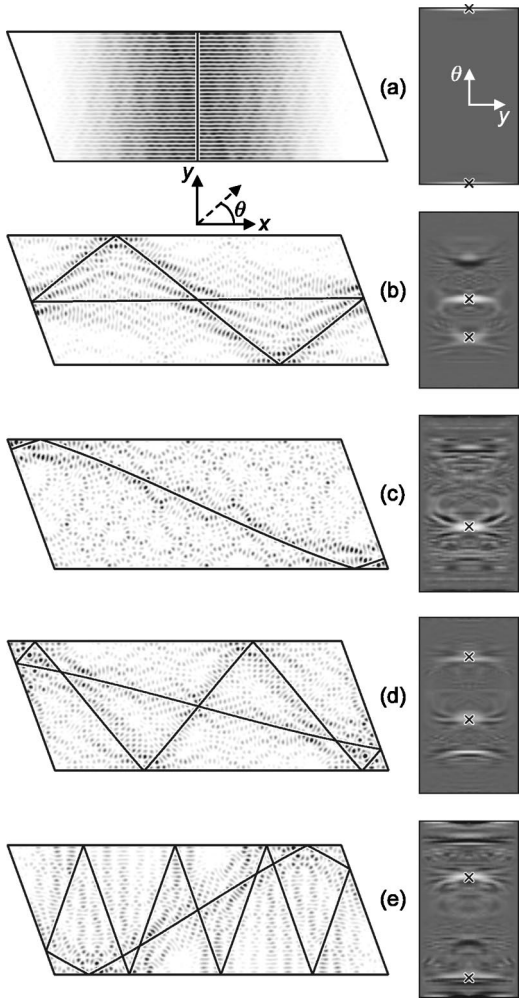

FIG. 7. (Left) Electric field intensity (white = 0) in x-y plane [axes shown below (a)] for eigenmodes of the $\beta = 20°$ cavity. Scarring ray paths are overlaid. (Right) Corresponding Wigner functions $\gamma(y,\theta)$ (black $\ll 0$, gray = 0, white $\gg 0$) with coordinate axes overlaid on (a). The coordinate ranges are -0.5 mm$< y <$ 0.5 mm and $0° < \theta < 90°$, as in Fig. 3. Crosses indicate initial coordinates of the scarring ray paths. The angular frequencies are: (a) 2.0426×10^{13} rad s^{-1}, (b) 2.0658×10^{13} rad s^{-1}, (c) 2.0200×10^{13} rad s^{-1}, (d) 2.0904×10^{13} rad s^{-1}, and (e) 2.0708×10^{13} rad s^{-1}.

(y,θ) (marked by crosses) of the corresponding scarring ray paths on the left of Fig. 7. This provides clear evidence that the scar patterns originate from these ray paths.

V. CONCLUSION

We have shown that effects analogous to quantum chaos occur in a 2D parallelogram-shaped cavity with an approximately parabolic refractive index profile and reflective walls. Such cavities could be made from commercially available GRIN lenses [7], which support 2D planar ray paths [6] as studied in this paper, as well as more complicated 3D paths. In our previous work [5] we have shown that, by partially silvering the end facets of the cavity, it is possible to probe the mode spectrum by observing Fabry–Pérot-like reso-

nances in transmission. In addition, we speculated that, by doping the GRIN material with luminescent erbium ions, it might be possible to image scarred modes directly at near optical frequencies. The major advantages of using optical, as opposed to semiconductor, systems to study quantum chaos-like effects are that they operate at room temperature and that lasers have extremely long coherence lengths, offering the potential for very high-resolution experimental studies. Such experiments could provide insights for understanding the properties of analogous quantum systems with mixed stable/chaotic dynamics which are of topical interest and beyond the scope of current theories [22]. Since GRIN materials are well developed and widely used in optoelectronics and telecommunications, they could provide a natural route to the technological exploitation of ray and wave chaos. For example, we have shown that the exponential sensitivity of ray paths in this system have the potential for applications as ultrafast optical switches or sensors [23].

ACKNOWLEDGMENTS

This work is supported by the UK Engineering and Physical Sciences Research Council (EPSRC). We are grateful to Dr. S. A. Brown for helpful discussions about erbium doping.

[1] E. J. Heller, Phys. Rev. Lett. **53**, 1515 (1984).
[2] S. Sridhar and E. J. Heller, Phys. Rev. A **46**, R1728 (1992); H.-J. Stöckmann, *Quantum Chaos: An Introduction* (Cambridge University Press, Cambridge, England, 1999).
[3] C. M. Marcus *et al.*, Phys. Rev. Lett. **69**, 506 (1992); J. P. Bird *et al.*, *ibid.* **82**, 4691 (1999).
[4] P. B. Wilkinson *et al.*, Nature (London) **380**, 608 (1996).
[5] P. B. Wilkinson *et al.*, Phys. Rev. Lett. **86**, 5466 (2001).
[6] J. A. Buck, *Fundamentals of Optical Fibers* (Wiley, New York, 1995).
[7] Lenses made from SELFOC glass, Nippon Sheet Glass Company Ltd., Type of lens: SLW 1.0 0.25 0.63 NC.
[8] M. Born and E. Wolf, *Principles of Optics*, 7th ed. (Cambridge University Press, Cambridge, England, 1999).
[9] J. U. Nöckel and A. D. Stone, Nature (London) **385**, 45 (1997); C. Gmachl *et al.*, Science **280**, 1556 (1998).
[10] A. Shudo *et al.*, Phys. Rev. E **49**, 3748 (1994).
[11] E. Ott, *Chaos in Dynamical Systems* (Cambridge University Press, Cambridge, England, 1993).
[12] The results of this section up to and including Eq.(10) are valid for an arbitrary choice of refractive index variation $n^2(x,y)$.
[13] P. B. Wilkinson *et al.*, Phys. Rev. E (to be published).
[14] B. Li and M. Robnik, J. Phys. A **27**, 5509 (1994).
[15] L. J. Slater, *Confluent Hypergeometric Functions* (Cambridge University Press, Cambridge, England, 1960)
[16] W. H. Press *et al.*, *Numerical Recipes*, 2nd ed. (Cambridge University Press, Cambridge, England, 1992).
[17] A. Kohler, G. H. M. Killesreiter, and R. Blümel, Phys. Rev. E **56**, 2691 (1997).
[18] T. A. Brody, Lett. Nuovo Cimento Soc. Ital. Fis. **7**, 482 (1973).
[19] H. Alt *et al.*, Phys. Rev. E **60**, 2851 (1999).
[20] P. Bellomo and T. Uzer, Phys. Rev. A **51**, 1669 (1995).
[21] P. A. Dando and T. S. Monteiro, J. Phys. B **27**, 2681 (1994).
[22] J. Main and G. Wunner, Phys. Rev. Lett. **82**, 3038 (1999).
[23] P. B. Wilkinson *et al.*, Physica B **272**, 484 (1999).